

Superwalking droplets

Rahil N. Valani^{1,*}, Anja C. Slim^{2,3}, and Tapio Simula^{1,4}

¹*School of Physics and Astronomy, Monash University, Victoria 3800, Australia*

²*School of Mathematical Sciences, Monash University, Victoria 3800, Australia*

³*School of Earth, Atmosphere and Environment, Monash University, Victoria 3800, Australia and*

⁴*Centre for Quantum and Optical Science, Swinburne University of Technology, Melbourne 3122, Australia*

A *walker* is a droplet of liquid that self-propels on the free surface of an oscillating bath of the same liquid through feedback between the droplet and its wave field. We have studied walking droplets in the presence of two driving frequencies and have observed a new class of walking droplets, which we coin *superwalkers*. Superwalkers may be more than double the size of the largest walkers, may travel at more than triple the speed of the fastest ones, and enable a plethora of novel few-droplet behaviors.

A liquid bath oscillating vertically may sustain bouncing droplets on its free surface [1]. For sufficiently large accelerations of the bath, these bouncing droplets may begin to walk [2]. Such walkers emerge just below the Faraday instability threshold, above which the liquid-air interface of the bath becomes unstable and standing subharmonic Faraday waves emerge [3]. In the walking state, the droplet is propelled by local Faraday waves that it excites on each bounce and whose decay time is a function of the proximity to the Faraday threshold, also referred to as the *memory* of the system. At high memory, waves generated by the droplet in the past continue to affect the motion of the droplet. Interactions of a walker with barriers and other droplets are mediated by this wave field, resulting in rich dynamics and a variety of few-droplet configurations [4–14]. This hydrodynamic system comprising a wave and a droplet mimics several features of the quantum realm including orbital quantization in rotating frames [15] and harmonic potentials [16, 17], wave-like statistical behavior in confined geometries [18, 19], tunneling across submerged barriers [20], and has been predicted to show anomalous two-droplet correlations [13]. A detailed review is provided by Bush [21]. Furthermore, this periodically driven wave-droplet entity is an example of a classical time crystal [22–24].

Walkers are typically driven by a pure sine wave $a_1(t) = \gamma \sin(2\pi ft)$, where γ is the amplitude of the driving acceleration, f is the driving frequency, and t is time. For a commonly studied system of silicone oil with 20 cSt viscosity and $f = 80$ Hz, droplet radii of 0.3 mm to 0.5 mm and walking speeds of up to 15 mm/s have been observed [25]. Here we present a new class of walking droplets, which we coin *superwalkers*, that emerge when the fluid bath is driven simultaneously at a frequency f and the subharmonic frequency $f/2$ with a phase difference $\Delta\phi$ according to the acceleration

$$a_2(t) = \gamma_f \sin(2\pi ft) + \gamma_{f/2} \sin(\pi ft + \Delta\phi). \quad (1)$$

In the commonly studied system noted above, superwalkers can be significantly larger than walkers with radii up to 1.4 mm and they can walk at up to 50 mm/s. The largest superwalkers undergo significant internal deformation

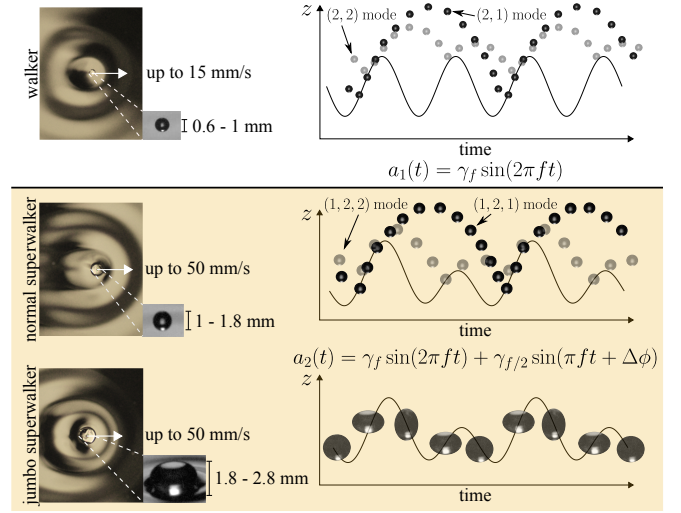


FIG. 1. Comparison of a walker (top), a normal superwalker (middle) and a jumbo superwalker (bottom). Superwalkers emerge when the bath is driven at two frequencies f and $f/2$ with a phase difference $\Delta\phi$. They may be significantly larger than walkers and may move significantly faster. Left panels show top views of typical droplets and their wave fields, and side views of the same droplets. Right panels show the bath motion (solid curve) and the typical bouncing motion of the droplets, see text for notation.

and barely lift off from the surface of the bath. We call these *jumbo superwalkers*. The key differences between a walker and the two kinds of superwalkers are summarized in the schematic of Fig. 1. Fundamental differences between walkers and superwalkers are also evident in their inter-droplet interactions. Due to their large inertia, superwalkers may easily overcome the wave barrier that typically prevents contact interactions between walking droplets, enabling superwalkers to form a variety of novel stationary and dynamic bound states.

Our experiments were performed using a circular bath of diameter 18 cm filled to a height of approximately 8 mm with silicone oil of viscosity 20 cSt. The bath was mounted on the cone of a subwoofer speaker [26], which was placed on an optical breadboard. Uniaxial vibra-

tions and leveling of the bath were ensured by observing uniform generation of Faraday waves [27]. Unless otherwise stated, the speaker cone was driven simultaneously at $f = 80$ Hz and $f/2 = 40$ Hz, with each driving signal fed into a separate voice coil. The acceleration of the bath was measured using two accelerometers mounted on the edges of the bath. For each accelerometer, the γ_{40} and γ_{80} acceleration amplitudes and phase shift $\Delta\phi$ were extracted through a nonlinear least squares fitting of the accelerometer signal to Eq. (1). The measured phase difference $\Delta\phi$ differed from the input value by a constant and has an uncertainty of $\pm 3^\circ$. The measured values of γ_f and $\gamma_{f/2}$ have an uncertainty of ± 0.05 g. Small droplets with radius less than 0.8 mm were created by swiftly extracting a needle from the oil bath while larger droplets were created using a syringe. The droplets were imaged with a top-view camera at 4 frames per second and with a side-view high-speed camera for a selection of cases at a typical frame rate of 4000 frames per second. A light panel placed above the camera provided sufficient illumination for the top-view images while a bright LED source illuminated the droplets from the side for the high-speed videos. The size of each droplet was measured from the top-view images using a Hough circle transform. Further details are provided in the Supplemental Material [28].

Characteristics of solitary superwalkers are shown in Figs 2 and 3. Figure 2(a) shows the speed of a droplet as a function of its radius for fixed values of γ_{80} and $\Delta\phi$ and three values of γ_{40} , illustrating the significant size and speed increase possible for superwalkers. Three prominent types of walking are observed for two-frequency driving and are identified in Fig. 2(a). The smallest droplets, which are walkers for single-frequency driving, become chaotic superwalkers upon adding the subharmonic driving signal. These droplets bounce aperiodically, see Fig. 2(b), and walk unsteadily with significant fluctuations in their velocities. Similar irregular walking dynamics for two-frequency forcing at 80 Hz and 64 Hz has been observed previously [29].

Much larger droplets that would not be able to walk for single-frequency driving can walk with two frequencies f and $f/2$. They have constant velocity and typically have greater speeds than the fastest walkers. Two different bouncing modes are realized for such superwalkers. We describe the vertical bouncing behavior of droplets driven by two frequencies using the generic notation (l,m,n) indicating that the droplet impacts the surface n times during m oscillation periods of the bath at frequency f , which equals l oscillation periods of the bath at frequency $f/2$. For single frequency driving, the l index is dropped. Superwalkers in the $(1,2,1)$ mode impact the bath once every two up-and-down motions of the bath as shown in Fig. 2(c) and their speed increases almost linearly with increasing size of the droplet. Surprisingly, despite the presence of γ_{40} being essential to the existence of super-

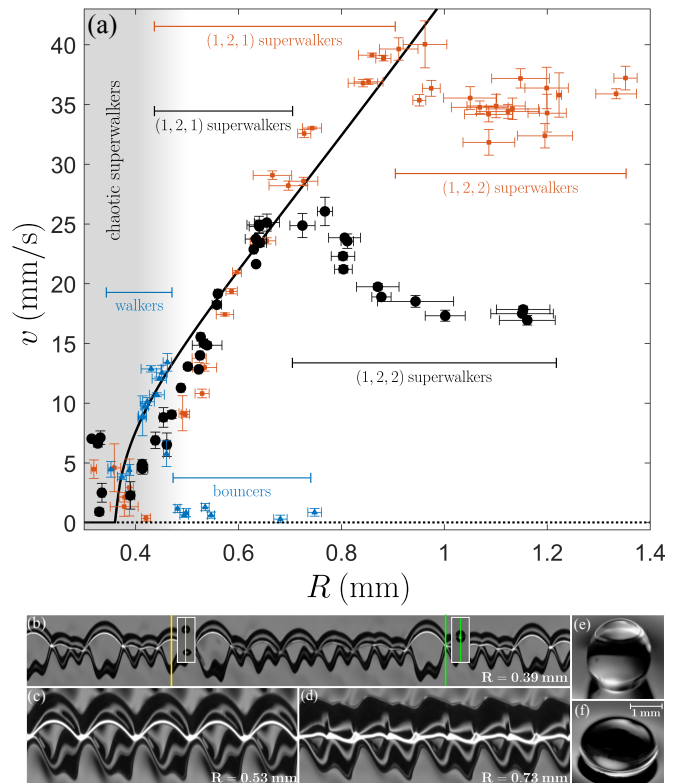


FIG. 2. Characteristics of a solitary superwalker. (a) Walking speed as a function of droplet radius for fixed values $\gamma_{80} = 3.8$ g and $\Delta\phi = 130^\circ$ and three different values of γ_{40} , specifically $\gamma_{40} = 0$ g (blue markers), $\gamma_{40} = 0.6$ g (black markers) and $\gamma_{40} = 1.0$ g (red markers). Details of the error bars and the theory prediction (solid curve) are explained in the Supplemental Material [28]. Three different bouncing behaviors are indicated for superwalkers: chaotic, $(1,2,1)$ and $(1,2,2)$. Vertical slice-time plots of droplets are shown for (b) chaotic, (c) $(1,2,1)$ and (d) $(1,2,2)$ bouncing modes corresponding to the black markers at the radii indicated. These ‘time crystal’ images are generated by juxtaposing vertical sections one pixel wide passing through the droplet’s center of mass. Panels (e) and (f) show the two extremes of the shape deformations of a jumbo superwalker.

walkers, its magnitude only marginally affects the speed of $(1,2,1)$ superwalkers. In fact, their speed compares well with a prediction for hypothetical single-frequency walkers of the equivalent size [28, 30].

Very large superwalkers bounce in a $(1,2,2)$ mode, see Fig. 2(d). In contrast to the $(1,2,1)$ superwalkers, the speed of $(1,2,2)$ superwalkers decreases with increasing droplet size. We attribute this behavior to the increased drag due to the prolonged contact time between the droplet and the bath. Superwalkers with radius $R \gtrsim 0.9$ mm undergo significant internal deformation and do not seem to lift off from the surface. We refer to these as *jumbo superwalkers*, see Figs 2(e,f) and Supplemental Video S1 [28]. The internal deformation of the jumbo superwalkers resonates with their $(1,2,2)$ bouncing, see

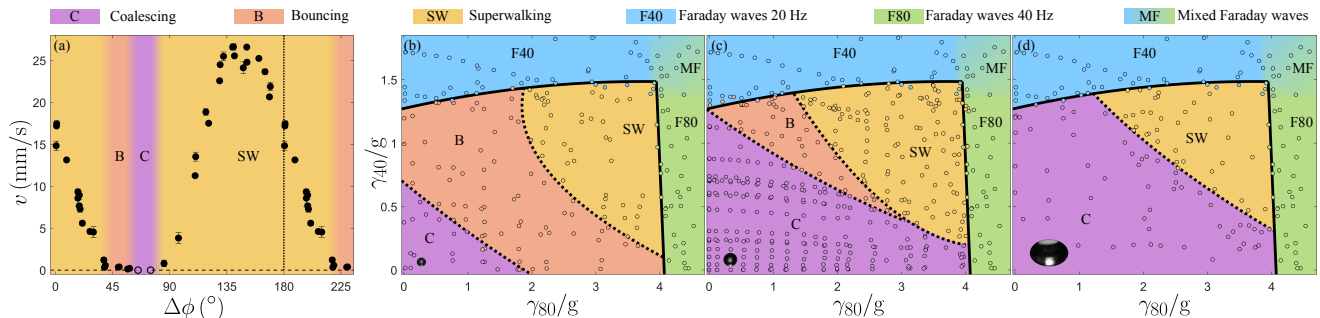


FIG. 3. (a) Droplet speed as a function of phase difference $\Delta\phi$ for a droplet of radius $R = 0.83 \pm 0.03$ mm for $\gamma_{80} = 3.8$ g and $\gamma_{40} = 0.6$ g. The data to the right of the vertical dashed line is repeated. Different behaviors occurring in the $(\gamma_{80}, \gamma_{40})/g$ parameter space for a fixed phase difference $\Delta\phi = 130^\circ$ and three different droplet radii: (b) $R = 0.6 \pm 0.05$ mm, (c) $R = 0.8 \pm 0.05$ mm, and (d) $R = 1.0 \pm 0.05$ mm. Error bars are explained in the Supplemental Material [28].

Figs 1. We find that jumbo superwalkers cannot simply bounce without walking, suggesting that a relative horizontal motion between such a droplet and the bath surface is needed for these droplets to exist. When the droplet size becomes too large, this is no longer possible and such droplets coalesce with the bath.

The value of the phase difference $\Delta\phi$ between the two driving signals crucially affects the behavior of droplets. Figure 3(a) shows representative data for the speed of a superwalker as a function of $\Delta\phi$ for fixed droplet radius and acceleration amplitudes. We find that superwalkers only exist for a limited range of phase difference and outside this range they either coalesce (open markers) or bounce. For the parameters corresponding to Fig. 3(a), the droplets bounce in a (1,2,2) mode both in the bouncing and the superwalking regime. The maximum speed occurs in the vicinity of $\Delta\phi \approx 140^\circ$, a value that does not appear to vary significantly with γ_{80} , γ_{40} , or droplet size.

Figures 3(b-d) show the different regimes observed in the $(\gamma_{80}, \gamma_{40})$ parameter space for a fixed phase difference $\Delta\phi = 130^\circ$ and three different droplet radii. Parametrically forcing a bath of liquid simultaneously at two different frequencies f and $f/2$ may result in a Faraday instability with either $f/2$ or $f/4$ waves depending on the amplitudes of the two frequencies and the phase difference $\Delta\phi$ between them [31]. We find that driving the bath at 80 Hz and 40 Hz delays the onset of 20 Hz Faraday waves when the driving acceleration γ_{80} is large. The onset of the 40 Hz Faraday waves is not significantly affected. For large γ_{40} and γ_{80} , both 40 Hz and 20 Hz Faraday waves appear to be excited simultaneously. Below the Faraday threshold, we find coalescing (C), bouncing (B), and superwalking (SW) regions with the extent of each region dependent on droplet size. For a relatively small droplet, Fig. 3(b), the extent of the bouncing and superwalking regions is large. The bouncing region progressively decreases with an increase in droplet size, see Figs 3(b-d). For a larger droplet, Fig. 3(d), the bouncing region disappears and the droplet may either coalesce or

walk. For even larger droplets, the superwalking region also vanishes. We also find that just above the 80 Hz-driving Faraday threshold, unlike walkers, superwalkers still walk steadily with their motion guided by the globally excited nonlinear Faraday waves. In the parameter regime where global Faraday waves are not excited, droplets always appear to trigger decaying 40 Hz Faraday waves, as illustrated by the similarity in wavelengths in Fig. 1.

Superwalkers open up an extended parameter space to explore new phenomena with walking droplets, a selection of which are illustrated in Fig. 4. Large two-component *bubble-droplets*, which are partly liquid and partly air, may be created with ease using a syringe filled with silicone oil and containing an air bubble. If the proportion of air is appreciable, then the bubble-droplet undergoes a pendulum motion, tumbling back and forth, see Fig. 4(a) and Supplemental Video S2 [28]. If the air only occupies a small proportion of the droplet, then the bubble-droplet walks much like a superwalker but at a reduced speed with respect to an air-free droplet.

Multiple superwalkers interacting with each other through their wave field form a variety of stationary and dynamic configurations. Two superwalkers can bind into a tight pair in which the droplets are separated only by a very thin air layer, see Fig. 4(b) and Supplemental Video S3 [28]. If such a pair of droplets have differing size they traverse a circular path, while a pair of identical droplets traverses a straight path. Similar states exist for staggered three-droplet and four-droplet configurations, see Figs 4(g,h) and Supplemental Videos S4 and S5 [28].

We have observed another type of bound pair called chasers, see Figs 4(c,d) and Supplemental Videos S6 and S7 [28], which have previously been found numerically for identical droplets with single-frequency driving [13, 32] and experimentally in an effectively one-dimensional annular geometry [33]. In this state, two droplets walk one behind the other at a constant speed. For droplets of differing size, the larger droplet leads and drags the smaller one in its wake. Chasing pairs of super-

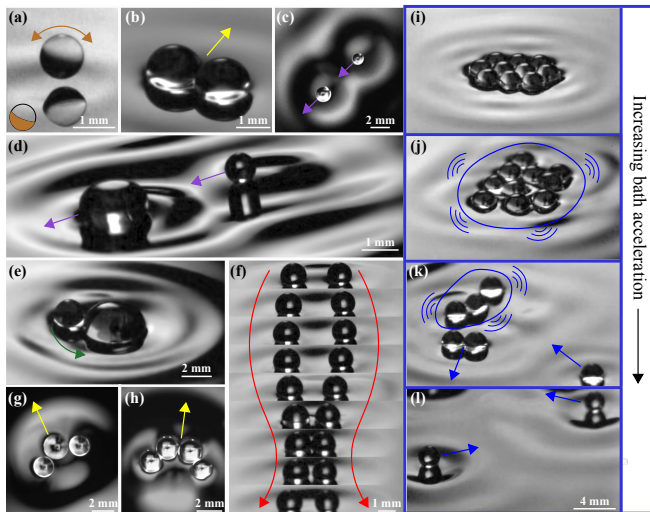


FIG. 4. A plethora of phenomena observed with superwalkers, see text for details.

walkers are robust and ubiquitous at high memory and the larger the size disparity between the two droplets, the more stably bound they are. Particularly disparate pairs can survive collisions with other droplets and even with the bath's walls. Less commonly, we have observed droplet trains consisting of three chasing droplets in descending size order. We note that chasing pairs are different from ratcheting pairs of walkers [12, 34]. Ratcheting motion typically occurs below the walking threshold and the pair travels slowly, while we find that chasers only appear at high memory and are an order of magnitude faster.

Two superwalkers also form a state reminiscent of promenading pairs of walkers, where the droplets walk in parallel with sideways oscillations [6, 7, 14]. Promenading pairs of walkers remain physically separated at all times due to the wave barrier formed as they approach one another. In contrast, promenading pairs of superwalkers undergo droplet-droplet collisions, bouncing off one another, see Fig. 4(f) and Supplemental Video S8. The center-of-mass of identical promenading superwalkers follows a straight path while that of even slightly mismatched superwalkers tends to follow a circular trajectory.

Two superwalkers may also form orbiting pairs similar to walkers. For mismatched sizes, such orbiting pairs may reverse their orbiting direction intermittently. With an extreme size imbalance, giant droplets that coalesce with the bath in isolation can persist if accompanied by a smaller orbiting satellite droplet, see Fig. 4(e) and Supplemental Video S9 [28].

When many superwalkers are present, the inter-droplet interactions favor crystalline droplet configurations for relatively low driving accelerations. If the value of γ_{40} is progressively increased while keeping γ_{80} fixed, see

Fig. 4(i-l), the crystal initially begins to jiggle, then starts to melt and ultimately the droplets evaporate and begin to superwalk at high speed, bouncing off each other elastically like billiard balls. This behavior is reminiscent of solid-liquid-gas phase transitions with the forcing amplitude acting as a temperature parameter, see Supplemental Video S10 [28]. These phenomena are robust with respect to interchanging the roles of γ_{40} and γ_{80} , and are associated with crossing the phase boundary between bouncing (B) and superwalking (SW).

Another interesting dynamical phenomenon may be observed when the forcing frequencies are slightly detuned, for example with 80 Hz and 39.5 Hz driving. Here the droplets perform a *stop-and-go motion* in which the droplets walk for a while, then stop abruptly, then walk again, and so on. This behavior is due to the driving signal that periodically traverses across the bouncing and superwalking regions. The result is an effective discrete-time dynamical system that emerges out of an underlying continuous-time system, see Supplemental Video S11 [28].

In conclusion, we have introduced a new class of walking droplets, coined superwalkers, enabled by adding a subharmonic driving signal to a periodically driven walking-droplet system. This introductory study of superwalkers paves the way for a wealth of new phenomena and warrants further investigation.

We are grateful to D. Duke, K. Helmerson, S. Johnstone, S. Morton, and L. Suryawinata for technical assistance and J.C. Miller for useful conversations. We acknowledge financial support from an Australian Government Research Training Program (RTP) Scholarship (R.V.) and the Australian Research Council via the Future Fellowship Project No. FT180100020 (T.S.).

* rahil.valani@monash.edu

- [1] J. Walker, *Sci. Am.* **238**, 123 (1978).
- [2] Y. Couder, E. Fort, C.-H. Gautier, and A. Boudaoud, *Phys. Rev. Lett.* **94**, 177801 (2005).
- [3] M. Faraday, *Phil. Trans. Roy. Soc. London Series I* **121**, 299 (1831).
- [4] G. Pucci, P. J. Sáenz, L. M. Faria, and J. W. M. Bush, *J. Fluid Mech.* **804**, R3 (2016).
- [5] S. Protière, A. Boudaoud, and Y. Couder, *J. Fluid Mech.* **554**, 85 (2006).
- [6] C. Borghesi, J. Moukhtar, M. Labousse, A. Eddi, E. Fort, and Y. Couder, *Phys. Rev. E* **90**, 063017 (2014).
- [7] J. Arbeláiz, A. U. Oza, and J. W. M. Bush, *Phys. Rev. Fluids* **3**, 013604 (2018).
- [8] S. Protière, S. Bohn, and Y. Couder, *Phys. Rev. E* **78**, 036204 (2008).
- [9] A. U. Oza, E. Siéfert, D. M. Harris, J. Moláček, and J. W. M. Bush, *Phys. Rev. Fluids* **2**, 053601 (2017).
- [10] S. I. Lieber, M. C. Hendershott, A. Pattanaporkratana, and J. E. MacLennan, *Phys. Rev. E* **75** (2007).
- [11] A. Eddi, A. Decelle, E. Fort, and Y. Couder, *Europhys.*

- Lett. **87**, 56002 (2009).
- [12] A. Eddi, D. Terwagne, E. Fort, and Y. Couder, Europhys. Lett. **82**, 44001 (2008).
- [13] R. N. Valani, A. C. Slim, and T. Simula, Chaos **28**, 096104 (2018).
- [14] R. N. Valani and A. C. Slim, Chaos **28**, 096114 (2018).
- [15] A. U. Oza, D. M. Harris, R. R. Rosales, and J. W. M. Bush, J. Fluid Mech. **744**, 404 (2014).
- [16] S. Perrard, M. Labousse, M. Miskin, E. Fort, and Y. Couder, Nat. Commun. **5**, 3219 (2014).
- [17] S. Perrard, M. Labousse, E. Fort, and Y. Couder, Phys. Rev. Lett. **113**, 104101 (2014).
- [18] D. M. Harris, J. Moukhtar, E. Fort, Y. Couder, and J. W. M. Bush, Phys. Rev. E **88**, 011001 (2013).
- [19] P. J. Sáenz, T. Cristea-Platon, and J. W. M. Bush, Nat. Phys. (2017).
- [20] A. Eddi, E. Fort, F. Moisy, and Y. Couder, Phys. Rev. Lett. **102**, 240401 (2009).
- [21] J. W. Bush, Annu. Rev. Fluid Mech. **47**, 269 (2015).
- [22] A. Shapere and F. Wilczek, Phys. Rev. Lett. **109**, 160402 (2012).
- [23] K. Sacha and J. Zakrzewski, Rep. Prog. Phys. **81**, 016401 (2018).
- [24] N. Y. Yao, C. Nayak, L. Balents, and M. P. Zaletel, arXiv:1801.02628 (2018).
- [25] J. Moláček and J. W. M. Bush, J. Fluid Mech. **727**, 612 (2013).
- [26] D. M. Harris, J. Quintela, V. Prost, P.-T. Brun, and J. W. M. Bush, Journal of Visualization **20**, 13 (2016).
- [27] D. M. Harris and J. W. M. Bush, J. Sound Vib. **334**, 255 (2015).
- [28] See Supplemental Material at [URL will be inserted by publisher] for videos of droplet dynamics, supplemental data and further technical details of the experiments.
- [29] N. Sampara and T. Gilet, Phys. Rev. E **94**, 053112 (2016).
- [30] A. U. Oza, R. R. Rosales, and J. W. M. Bush, J. Fluid Mech. **737**, 552 (2013).
- [31] H. W. Müller, Phys. Rev. Lett. **71**, 3287 (1993).
- [32] M. Durey and P. A. Milewski, J. Fluid Mech. **821**, 296329 (2017).
- [33] B. Filoux, M. Hubert, and N. Vandewalle, Phys. Rev. E **92**, 041004 (2015).
- [34] C. A. Galeano-Rios, M. M. P. Couchman, P. Caldaïrou, and J. W. M. Bush, Chaos **28**, 096112 (2018).

FURTHER DETAILS OF THE EXPERIMENTS

Our experiments used silicone oil of nominal viscosity 20 cSt and density 950 kg/m³ at 25°C. A circular bath of diameter 18 cm was filled to a height of approximately 8 mm with the oil. The bath had a circular aluminium base of diameter 218 mm and thickness 6 mm with a 3D-printed annular ring adhesively bonded to it to form the vertical wall. The bath was mounted on a subwoofer speaker cone [26] (UM12-22 12" Ultimax DVC Subwoofer 2 ohms Per Coil) that was placed on an optical breadboard. We verified that the subwoofer acceleration axis was vertical with lateral vibrations less than 5% of the vertical vibrations. The bath was adjusted within the cone so that Faraday waves were generated uniformly on its surface [27]. Once this adjustment was complete, the bath was epoxied in place.

The speaker cone was driven simultaneously at frequencies f and $f/2$ via two independent voice coils at a prescribed phase shift. Superwalkers were observed for driving frequencies 50 Hz $\lesssim f \lesssim$ 100 Hz. For our detailed investigation reported on in the main text, we used $f = 80$ Hz. The two voice coils were driven by connecting them to an amplifier (Crown XLS1002 Drivecore, 1100 W), which in turn was connected to a computer running the audio editing software Audacity to generate the driving signals. The acceleration of the bath was measured using two horizontally mounted, diametrically opposed accelerometers (MPU6050 Module 3 Axis Gyroscope + Accelerometer) on the annular ring. These accelerometers were connected to the same computer using an Arduino UNO microcontroller. For each accelerometer, the γ_{40} and γ_{80} acceleration amplitudes and phase shift $\Delta\phi$ were extracted using nonlinear least square fitting of the measured accelerometer signal to the expression $\gamma_f \sin(2\pi ft) + \gamma_{f/2} \sin(\pi ft + \Delta\phi)$, Eq. (1) in the main text. A Fourier transform of the signals was also used to verify that there was no significant power at spurious frequencies. The measured peak acceleration amplitude decayed over time, presumably due to the Ohmic heating of the copper in the voice coils. For collecting several data sets at the same acceleration, a feedback loop was used to adjust the amplitude of the input signal based on the measured amplitude using the past 2 seconds of accelerometer readings. Adjustments to the input signal were made approximately every 10 seconds, much quicker than the time scale of decay of approximately 1 – 2 minutes. This was sufficient to maintain the accelerations within ± 0.05 g. The measured phase difference from the accelerometer $\Delta\phi$ differed from the input phase difference by a constant value, presumably due to damping inherent to this periodically driven oscillator. The uncertainty in the measured phase difference of approximately $\pm 3^\circ$ was calculated as the difference between the phase readings of the two diametrically opposed accelerometers. We found

that the speaker heated up over time, raising the temperature of the silicone oil. This altered its viscosity and decreased the Faraday threshold. Therefore, the temperature of the oil was measured using a thermocouple and it was kept in the range 21-23°C by limiting the time of each experimental run to approximately 20 minutes. This limited the variability in the Faraday threshold to within approximately 0.1 g, which is comparable to the uncertainty permitted in the feedback loop.

Small droplets with radius less than 0.8 mm were created by swiftly extracting a needle from the oil bath while larger droplets with radius greater than 0.8 mm were created using a syringe with needles of different diameters. The droplet's horizontal motion was recorded from above using a Nikon D90 DSLR camera in burst mode at 4 frames per second. Typically 4-8 images were taken of a droplet walking in a straight line, which were then used to determine the size and the speed of the droplet. High speed videos of the droplets were taken using Chronos 1.4 high-speed camera in order to determine the bouncing mode of a single droplet and visualize many droplet dynamics at a typical frame rate of 4000 frames per second. A Phantom VEO 640 high-speed camera was used to visualize the large internal deformations of a jumbo superwalker. An LED panel placed above the camera provided sufficient illumination for the overhead images while another LED source illuminated the droplets from the side for the videos taken using the high-speed camera. The size of a droplet was measured from the overhead images using a Hough circle transform implemented in Matlab and was taken as the average value from the overhead burst sequence. The speed was calculated as the total distance that the centre of the droplet traveled divided by the duration of the burst sequence.

The superwalkers were not affected significantly by the ambient air currents, presumably due to their large inertia. Nevertheless, the experiments were performed under a shroud to protect the smaller droplets from spurious drifting due to air currents.

We measured the Faraday threshold for single-frequency forcing at 80 Hz as $\gamma_{F80} \approx 4.2$ g and for single-frequency forcing at 40 Hz as $\gamma_{F40} \approx 1.3$ g. We observed that for a fixed moderate value of γ_{40} , as γ_{80} is increased progressively, circular concentric waves start forming at the edges of the bath with their radial extent increasing as γ_{F80} is approached from below. This results in the superwalkers becoming confined, and walking along the edges of the bath. We note that such waves did not form with single-frequency forcing either for 40 Hz or 80 Hz.

Error estimation

In Fig. 2(a) of the main text and the Supplemental Figs 5 and 6, each point represents the observed data for a single droplet with size and speed error bars given by the

standard deviation calculated from the given droplet's burst sequence. For larger superwalkers, the error in the size is greater because internal deformation of the droplet causes appreciable variations in its radius. The spread of data in these figures provides an indication of the uncertainty in the acceleration amplitude of the bath.

In Fig. 3 of the main text and Supplemental Fig. 7, each point again represents the data for a single droplet. The stated error in the droplet's radius is the standard deviation of all the droplets' radii. The error bars in the droplets' speed in Fig. 3(a) of the main text and Fig. 7, are the standard deviation calculated from the given droplet's burst sequence. The spread of data in these figures provides an indication of the uncertainty in the acceleration amplitude of the bath.

FURTHER CHARACTERIZATION OF THE DYNAMICS OF A SOLITARY SUPERWALKER

Figure 5(a) provides an extension of the results presented in Fig. 2(a) of the main text. The theory curve is the predicted speed-size relationship for a (2,1) walker with single-frequency driving using the Oza-Rosales-Bush stroboscopic model (see equation (4.2) of [30]). For the model, we set the adjustable parameters of the impact phase and the non-dimensional drag coefficient as $\sin(\Phi) = 0.2$ and $C = 0.17$ respectively. For the accelerations, we use only the γ_{80} value and the γ_{F80} Faraday threshold value. All other parameters are specified from the experimental conditions. Surprisingly, this curve accurately captures the speed of (1,2,1) superwalkers, despite not having explicit dependence on the value of γ_{40} . Figure 5(b) provides further insight into the relationship between the speed and the intensity of the subharmonic driving for four different-sized droplets. The smallest droplet ($R = 0.45$ mm) is a (2,1) walker for single-frequency driving. Adding the subharmonic frequency barely impacts its speed up to a threshold γ_{40} value, beyond which the speed drops precipitously and the droplet switches to a chaotic mode. A slightly larger droplet of $R = 0.63$ mm is a bouncer for a single-frequency driving and remains so for small γ_{40} . Beyond a threshold γ_{40} value, the droplet begins to walk and does so with increasing speed before plateauing for moderately large γ_{40} . A medium-sized droplet of $R = 0.77$ mm exhibits similar behaviour but its speed continues to increase with γ_{40} . The largest droplet of $R = 1.16$ mm coalesces at low γ_{40} and directly begins to superwalk after a threshold value of γ_{40} with its speed increasing linearly with γ_{40} and can reach a speed of 50 mm/s.

To complement Fig. 2(a) in the main text, Fig. 6(a) shows the speed of a solitary droplet as a function of its radius for fixed γ_{40} and $\Delta\phi$ and three different values of γ_{80} . We find that increasing γ_{80} results in an increased speed for steadily walking superwalkers. Fig-

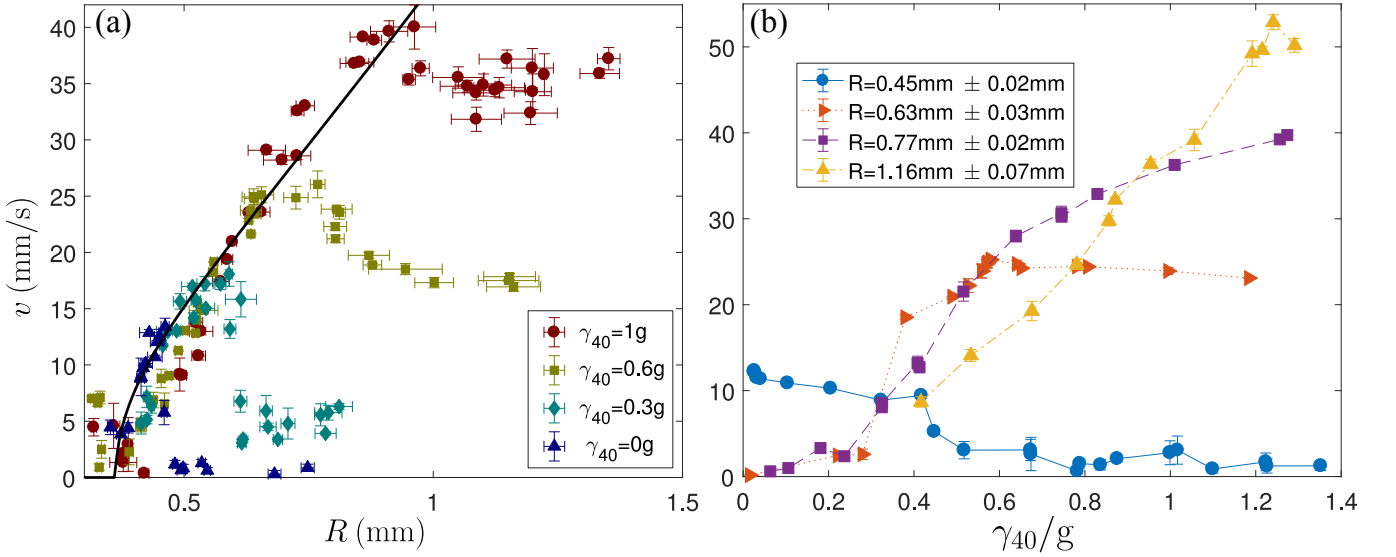


FIG. 5. Characteristics of a solitary superwalker for fixed $\gamma_{80} = 3.8$ g and fixed $\Delta\phi = 130^\circ$. (a) Speed as a function of radius for $\gamma_{40} = 0$ g, 0.3 g, 0.6 g, and 1 g. The black curve is the prediction from the stroboscopic model for single-frequency walkers [30]. (b) Speed as a function of γ_{40} for droplet radii $R = 0.45$ mm, $R = 0.63$ mm, $R = 0.77$ mm, and $R = 1.16$ mm. Note that the data in frames (a) and (b) correspond to orthogonal slices through the same three dimensional (v, R, γ_{40}) parameter space.

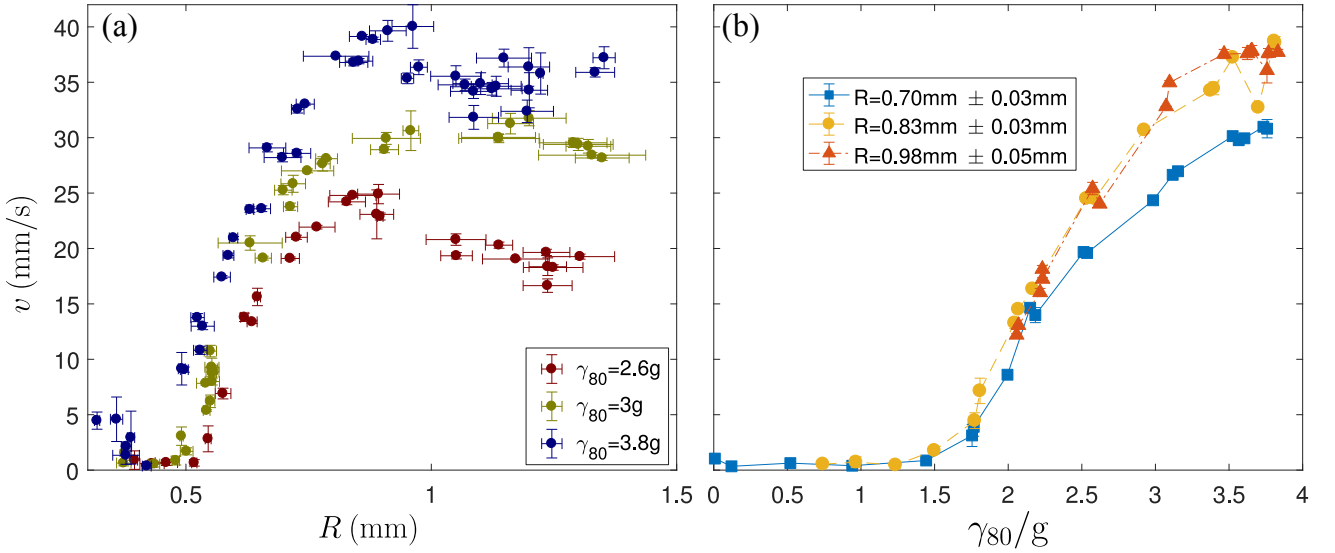


FIG. 6. Characteristics of solitary superwalkers for fixed $\gamma_{40} = 1$ g and fixed $\Delta\phi = 130^\circ$. (a) Speed as a function of radius for $\gamma_{80} = 2.6$ g, 3 g, and 3.8 g. (b) Speed as a function of γ_{80} for droplet radii $R = 0.70$ mm, $R = 0.83$ mm, and $R = 0.98$ mm. Coalescence occurs in the case of $R = 0.83$ mm for $\gamma_{80} \lesssim 0.6$ g and in the case of $R = 0.98$ mm for $\gamma_{80} \lesssim 2.0$ g. Note that the data in frames (a) and (b) correspond to orthogonal slices through the same three dimensional (v, R, γ_{80}) parameter space.

ure 6(b) shows the speed as a function of γ_{80} for three different droplet radii. The trend for all three droplet sizes is similar. We note that the largest droplet, a jumbo superwalker, only exists in the superwalking regime and coalesces at lower γ_{80} .

Figure 7 shows additional data for the speed of a droplet as a function of the phase difference $\Delta\phi$ for fixed γ_{80} and γ_{40} and two different radii of $R = 0.54$ mm and $R = 0.60$ mm, smaller than the droplet size for which

data is presented in the main text. For both these smaller droplets, the coalescence region vanishes. In the bouncing region, the smaller droplet bounces chaotically while the slightly larger droplet bounces in a $(1,2,2)$ mode. At the edges of the superwalking region, both sizes of droplets bounce in a $(1,2,2)$ mode, while at the peak of the superwalking region, both bounce in a $(1,2,1)$ mode.

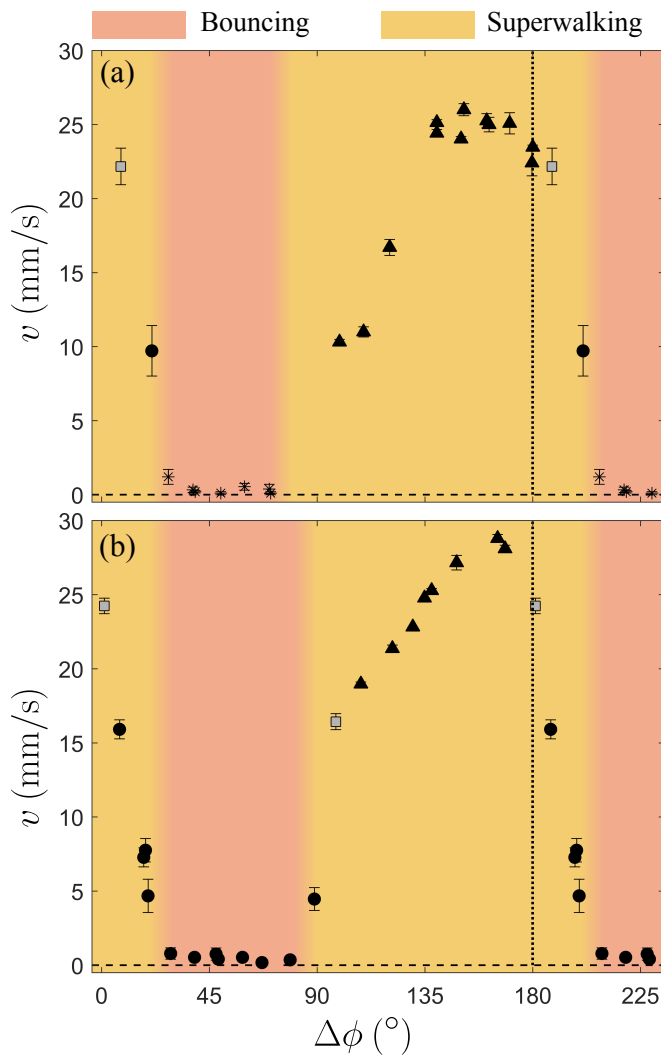


FIG. 7. Droplet behavior as a function of the phase difference $\Delta\phi$ is shown at fixed driving acceleration amplitudes $\gamma_{80} = 3.8g$ and $\gamma_{40} = 0.6g$ for droplets of radii (a) $R = 0.54 \pm 0.03$ mm and (b) $R = 0.60 \pm 0.02$ mm. A (1,2,2) bouncing mode is shown as black filled circles, a (1,2,1) bouncing mode is shown as gray squares and transition between (1,2,1) and (1,2,2) is shown as black filled triangles and chaotic bouncing is shown as black asterisks. The data to the right of the vertical dashed line is repeated.

SUPPLEMENTAL VIDEOS

Supplemental Video S1: Bouncing and walking motion of a jumbo superwalker (recorded at 4000 fps and encoded at 60 fps) of radius $R = 1.2$ mm at $\gamma_{80} = 3.8g$, $\gamma_{40} = 0.6g$, and $\Delta\phi = 130^\circ$. The droplet undergoes large internal deformations and hardly lifts off from the surface.

Supplemental Video S2: Bubble-droplet (recorded at 4000 fps and encoded at 60 fps) of radius $R = 0.6$ mm at $\gamma_{80} = 3.8g$, $\gamma_{40} = 1g$, and $\Delta\phi = 130^\circ$. The bubble-

droplet undergoes a pendulum motion, tumbling back and forth.

Supplemental Video S3: Tightly bound pair of identical droplets (recorded at 4000 fps) with radius $R = 0.82$ mm at $\gamma_{80} = 2.6g$, $\gamma_{40} = 0.5g$, and $\Delta\phi = 130^\circ$. This tight pair traverses a straight path. The start of the video is encoded at 60 fps to show the bouncing motion and the remaining part is encoded at 420 fps to show the walking motion.

Supplemental Video S4: Tightly bound triplet of identical droplets in a staggered configuration (recorded at 4000 fps) with radius $R = 0.80$ mm at $\gamma_{80} = 2.6g$, $\gamma_{40} = 0.5g$, and $\Delta\phi = 130^\circ$. The three droplets walk in a straight line at constant speed in a staggered configuration with the central droplet in the lead and the outer droplets trailing. The start of the video is encoded at 60 fps to show the bouncing motion and the remaining part is encoded at 300 fps to show the walking motion.

Supplemental Video S5: Tightly bound quadruplet of identical droplets in a staggered configuration (recorded at 4000 fps and encoded at 420 fps) with radius $R = 0.81$ mm at $\gamma_{80} = 2.6g$, $\gamma_{40} = 0.5g$, and $\Delta\phi = 130^\circ$. The four droplets walk in a straight line at constant speed in a staggered configuration with the droplets forming an arc.

Supplemental Video S6: Chasing pair of superwalkers (recorded at 4000 fps and encoded at 60 fps) with a large difference in size between the leading droplet ($R = 1.0$ mm) and the trailing droplet ($R = 0.53$ mm) at $\gamma_{80} = 3.8g$, $\gamma_{40} = 1g$, and $\Delta\phi = 130^\circ$.

Supplemental Video S7: Chasing pair of superwalkers (recorded at 4000 fps and encoded at 60 fps) with a relatively small size difference between the leading droplet ($R = 0.74$ mm) and the trailing droplet ($R = 0.64$ mm) at $\gamma_{80} = 3g$, $\gamma_{40} = 0.9g$, and $\Delta\phi = 130^\circ$.

Supplemental Video S8: Promenading pair of superwalkers (recorded at 4000 fps and encoded at 420 fps) with radius $R = 0.95$ mm at $\gamma_{80} = 2.6g$, $\gamma_{40} = 0.8g$, and $\Delta\phi = 130^\circ$. The droplets collide and bounce off each other in each cycle.

Supplemental Video S9: Giant droplet (recorded at 4000 fps and encoded at 60 fps) of radius $R = 2$ mm with an accompanying orbiting satellite droplet of radius $R = 1$ mm at $\gamma_{80} = 2.9g$, $\gamma_{40} = 0.8g$, and $\Delta\phi = 130^\circ$. The giant droplet would coalesce in isolation but persists in the presence of the orbiting satellite droplet.

Supplemental Video S10: Self-organization of

many droplets (recorded and encoded at the strobing frequency of 40 fps). Many identical droplets of radii $R = 0.8$ mm form a crystalline bound state at $\gamma_{80} = 2.1$ g, $\gamma_{40} = 0.4$ g and $\Delta\phi = 130^\circ$. The stationary crystal starts jiggling, with the individual droplets moving around within the bound crystal as γ_{40} is increased to 0.7 g. As γ_{40} is increased further to 0.9 g, the bound crystal disintegrates but two- and three-droplet bound

states may remain. At an even higher γ_{40} of 1.1 g, the superwalkers achieve high speed and collide with each other much like an ideal gas.

Supplemental Video S11: Stop-and-go motion of droplets (recorded at 120 fps and encoded at 240 fps) with frequencies 80 Hz and 39.5 Hz at $\gamma_{80} = 3$ g, $\gamma_{39.5} = 1$ g, and $\Delta\phi = 130^\circ$.